Application of nano-particle coatings to carrier particles using an integrated fluidized bed supercritical fluid precipitation process

Leeke, Gary A.; Lu, Tiejun; Bridson, Rachel H.; Seville, Jonathan P.k.

DOI:
10.1016/j.supflu.2014.03.012

Document Version
Publisher's PDF, also known as Version of record

Citation for published version (Harvard):
Leeke, GA, Lu, T, Bridson, RH & Seville, JPK 2014, 'Application of nano-particle coatings to carrier particles using an integrated fluidized bed supercritical fluid precipitation process', *Journal of Supercritical Fluids*, vol. 91, pp. 7-14. https://doi.org/10.1016/j.supflu.2014.03.012

J. of Supercritical Fluids 91 (2014) 7–14

Contents lists available at ScienceDirect

The Journal of Supercritical Fluids

journal homepage: www.elsevier.com/locate/supflu

Application of nano-particle coatings to carrier particles using an integrated fluidized bed supercritical fluid precipitation process

Gary A. Leeke[a,*], Tiejun Lu[a], Rachel H. Bridson[a], Jonathan P.K. Seville[b]

[a] Centre for Formulation Engineering, School of Chemical Engineering, University of Birmingham, Birmingham B15 2TT, UK
[b] Department of Chemical and Process Engineering, University of Surrey, Guildford, Surrey GU2 7XH, UK

ARTICLE INFO

Article history:
Received 5 August 2013
Received in revised form 26 March 2014
Accepted 27 March 2014
Available online 4 April 2014

Keywords:
Supercritical fluid
Fluidized bed
Wurster coater
Coating
Nano-particles
Excipient
Dosage form

ABSTRACT

Production of active ingredients such as pharmaceuticals in nano-particulate form is highly desirable but the resulting product is difficult to handle and to use in applications. A novel process is described for coating nanoparticles onto excipient particles of c. 300 μm by rapid expansion of a supercritical solution (RESS) into two types of modified proprietary equipment: a Wurster coater and a fluidized bed. This novel approach has been demonstrated through the successful deposition of six mimics for active ingredients (benzoic acid, adamantane, ferrocene, phenanthrene, stearic acid and vitamin K3) on carrier excipient particles of microcrystalline cellulose (MCC). Evidence from SEM, EDX and Confocal Raman microscopy suggests that the coating particles are below 30 nm in size. Unlike most conventional coating processes, this approach avoids the use of liquids and high temperatures. As a wide range of actives and excipients can potentially be employed, the approach is applicable across the process and product industries, in particular pharmaceutical, household goods, personal care and catalyst industries.

1. Introduction

Active ingredients in nanoparticulate form can have advantageous properties; for example, nanoparticulate drugs can show higher bioavailability [1] and catalysts higher activity [2]. Nanoparticulates are not readily attainable through conventional crystallization routes and a subsequent comminution stage is often necessary, which may disadvantageously alter the physicochemical properties of the product. In principle, supercritical processes are more attractive because they can deliver a narrow particle size distribution [3,4], consist of only one process step, do not require liquid solvents and can be undertaken at moderate temperatures. A further advantage is that they offer control over solid state properties, producing either amorphous or crystalline material and sometimes polymorphs which are not obtainable by other means [5,6].

The supercritical particle formation process used here is rapid expansion of supercritical solutions (RESS), in which the solution is expanded through a constriction, resulting in a very rapid pressure decrease, high supersaturation and rapid precipitation of fine particles. There are numerous reports describing the production of nanoparticles via this method [7–12]. However, since even van der Waals' forces between particles of 1 μm far exceed the weight of the individual particles [13], such powders are very cohesive and cannot easily be processed without extensive further treatment. Additionally, nucleation in the expanding RESS jet occurs very close to the origin of the jet [14] and it is therefore difficult to prevent agglomeration from occurring before any stabilization treatment can be applied; indeed, evidence from other workers [15] suggests that the RESS product is usually in aggregated form. It would be advantageous, therefore, to capture and preserve the active particles close to their origin, for subsequent processing or re-dispersion. Fluidized beds are widely used in the chemical process and pharmaceutical industries as reactors, mixers, dryers, agglomerators and coaters [16]. Fluidization occurs when an upward flow of fluid passing through a bed of particles becomes sufficient to support them against gravity. The pressure drop across the bed then equals the bed weight and the particles are free to move. At this point (the point of incipient or minimum fluidization) the bed is said to be fluidized. With good design, mixing in fluidized beds is very rapid, the bed is nearly isothermal and high rates of heat and mass transfer can be attained. The applications of fluidized beds that are of relevance here are (1) coating, e.g. of pharmaceutical products, particularly pellets and tablets [17] and (2) filtration, where fine (0.5–10 μm) particles can be captured on larger fluidized carrier particles e.g. to remove environmentally-damaging and health-threatening particles from dirty gas streams passed upwards through a fluidized bed [18]. By injecting a RESS jet directly into a fluidized bed of carrier excipient

* Corresponding author. Tel.: +44 1214145351.
E-mail address: g.a.leeke@bham.ac.uk (G.A. Leeke).

http://dx.doi.org/10.1016/j.supflu.2014.03.012
0896-8446/

particles, these two concepts can be combined to allow nanoparticulate coating of active material onto excipient particles. The immediate collection of nanoparticles from a RESS process, close to their point of origin, would prevent their further growth and agglomeration, so forming a product which captures and retains the efficacy and special features of the nanometer size in an easily handleable form. The capture of particles in this way also provides a means of alleviating concerns relating to the inappropriate escape of very small particles into the environment. In contrast to conventional fluidized bed coating, this strategy also avoids the use of liquids.

There have been previously reported attempts at using supercritical fluids to coat particles, but, to the authors' knowledge, none using the approach outlined above. Kim et al. [19] and Mishima et al. [20] used RESS to encapsulate active substances in polymer particles by dissolving both components in supercritical-CO_2 and co-precipitating the mixture. Bertucco and Vaccaro [21] used anti-solvent methods for encapsulation from a suspension of particles in conventional solvents, while composite particles have also been produced by the supercritical anti-solvent technique [22,23]. Wang et al. [24] used the RESS technique to precipitate PVC covinyl acetate and hydroxypropyl cellulose onto 315 and 500 μm glass spheres placed in a collector vessel held at a pressure and temperature intermediate between supercritical and ambient. They also added acetone to the CO_2 in order to enhance solubility of the polymer. The coating quality varied from smooth, when the polymer contacted the glass surface in a liquid state, to particulate, when precipitation occurred prior to contact. Tsutsumi et al. [25] and Wang et al. [26] expanded a RESS jet through a nozzle into a bed fluidized with air, and deposited a smooth paraffin coating onto 56 μm catalyst particles and 1 μm SiO_2, respectively. Schreiber et al. [27,28] coated various particles with paraffins by expanding supercritical solutions into a bed at high pressure fluidized with carbon dioxide. Krober and Teipel [29] coated glass beads with stearyl alcohol in a similar manner.

The work reported here is distinct from previous studies in that it is aimed exclusively at production of nanoparticles and their capture onto larger carriers which are freely fluidizable and suitable for subsequent handling.

2. Materials and methods

2.1. Materials

All materials were used as purchased without further purification: liquid carbon dioxide (≥99.8%) [BOC, UK]; benzoic acid S.L.R. (≥99.5%) [Fisons, UK]; methanol (≥99.6% GC) [Sigma–Aldrich, UK]; microcrystalline cellulose (MCC, 295 μm in diameter) in near-spherical particulate form ["Ethispheres", NP Pharm, France]. Six chemical compounds, each with adequate solubility in supercritical CO_2, were selected as mimic active ingredients [all supplied by Sigma–Aldrich, UK]: adamantane (≥99%), ferrocene (≥98%), stearic acid (≥95%), phenanthrene (98%) and vitamin K3 (≥98%). Throughout the remaining text, these compounds and benzoic acid are referred to as the 'actives'.

2.2. Equipment

A schematic representation of the RESS equipment is given in Fig. 1. Further details of the equipment are described in Section 2.3. Two different RESS-fluidized bed combinations were explored, one of a conical-cylindrical Wurster-type geometry (RESS-WTS) and one based on a cylindrical geometry operating as a bubbling fluidized bed (RESS-BFB) (Fig. 1).

In the Wurster configuration, the coating solution or suspension is normally injected upwards into the bed at the base by means of a two-fluid nozzle and the central jet breaks through the surface of the bed. The fluidizing gas also enters through the distributor at the base – which is usually some form of perforated or otherwise porous plate – and the excess gas at the centre of the bed ensures that particle circulation is up in the centre in the "spout" region and down near the walls. It is common to insert a cylindrical "draft tube", as shown in Fig. 1, to encourage this circulation and to ensure that particles enter the spout near the base and so pass through the coating region. It is also common for the bed walls to be conical or conical/cylindrical in shape, again to enhance circulation. Further details of the Wurster system are given by Palmer et al. [30]. In the bubbling fluidized bed, the coating fluid mixture is also injected through the base but the jet is completely submerged and the particle circulation is less strong.

2.3. The RESS process

Liquid CO_2 was withdrawn from a gas cylinder and pre-cooled in a cold bath (Grant UK W14 + C1G) to around 0 °C to prevent cavitation in the air driven liquid pump (Haskel MS-71, Haskel, USA) that was used to compress the CO_2 to the desired working pressure of *c.* 100 bar. The pressure was maintained to an accuracy of ±0.5 bar using a back pressure regulator, BPR (Tescom26-1762-24, Tescom Europe, Germany). Compressed CO_2 was brought to the desired temperature (40 °C) by heating in a heat exchanger, HE (Tecam bath + Grant ZA serial heater, UK). The flow of CO_2 was measured using a high pressure fluid mass flow metre, MF (coriolis type; RHE08, Rheonik, Germany) and entered the half litre high pressure vessel, PV (Baskerville BS5500 CAT1, UK). The vessel was 180 mm in depth, 60 mm in diameter and equipped with a hot water jacket to maintain the desired temperature. In the vessel, CO_2 was contacted with the pre-charged active compound causing it to dissolve into the CO_2 stream. The active compound was placed in a tubular glass sample holder which was sealed at the base with a 15 μm pore glass sinter to ensure that no solid particles were entrained in the CO_2 stream. 10–30 g active powder, more than three times the consumption of one typical test, was charged into the sample holder to form a 30–40 mm fixed bed. The loaded sample holder was located in the vessel in a position that covered the exit port to force the CO_2 stream to pass through the bed before it left the vessel and entered the nozzle. Upon leaving the vessel, the CO_2 stream was nearly saturated with the active compound. The concentration of the CO_2 solution was monitored in-line using a high pressure UV detector (UV-2075 plus, Jasco, Japan), which was calibrated against standard solutions. From this point, the CO_2 solution was introduced (as described below) either into the RESS-BFB or into the RESS-WTS, in order to coat the actives onto the MCC excipient particles fluidized within them.

2.4. Coating with the RESS-WTS

Compressed air that had been heated to 35 °C with an in-line heater (CAST X 500, Watson Marlow, UK) was introduced to the bottom of the fluidization apparatus that had been charged with 30 g of MCC particles. The air flow rate was just above that required for incipient fluidization (U_{mf}) which was obtained by a test using only MCC particles and hot air in the Wurster coater. Valve V1 was opened to let pure CO_2 join the air to fluidize the MCC. After fluidization had been initiated, valve V1 was closed and V2 was opened simultaneously to allow introduction of the solute-laden CO_2 solution (produced in Section 2.3) into the RESS-WTS apparatus. The solution was jetted upward in the same direction as the air flow via a 102 μm diameter sapphire nozzle into the bed of excipient. The nozzle was located in the centre of the air distributor at the

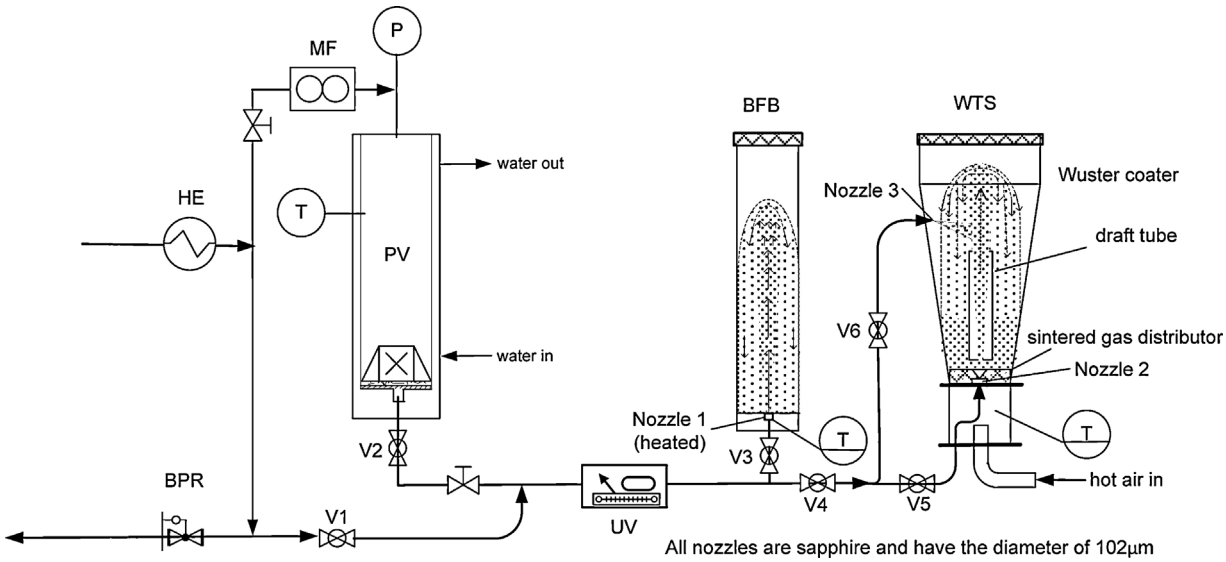

Fig. 1. Schematic representation of the RESS-apparatus showing both WTS and BFB units.

bottom of the Wurster coater where the solution sprayed into the bed as in a standard Wurster coater. The CO_2 mass flow rate depends on its pre-nozzle pressure and temperature, nozzle size and nozzle conditions. The nozzle diameter was kept constant at 102 μm. Under some conditions, solid precipitated in and around the nozzle caused partial blocking. The CO_2 flow rate measured in this work ranged from 12 to 311 g/min. Particles of the active precipitated from the RESS jet were brought into contact with the fluidized MCC carrier particles, where they formed a coat. Simultaneously, CO_2 pressure dropped to ambient and the CO_2 changed from supercritical states to gas and mixed with the air to fluidize the MCC particles. After a designated coating time, from 5 to 118 min, the CO_2 + active solution pipeline was purged with pure CO_2, while the particles remained fluidized for 5–10 min; their surfaces were unaffected during this time, as indicated by SEM images (not included here). The coated MCC particles were collected and kept in air-tight sample bottles for further characterization and analysis (see Section 2.6).

2.5. Coating with the RESS-BFB

This coating method is similar to the RESS-WTS but utilizes a fluidized MCC bed in a cylindrical container operating as a bubbling fluidized bed. It uses no air but only RESS CO_2 to fluidize the bed. A nozzle heater (nozzle 1) and temperature controller were installed and heated to approximately 60 °C to minimize dry ice formation and nozzle blockage. Prior to passing CO_2 through the cylindrical fluidized bed, 40–60 g of MCC particles were added to give respective bed heights of either 70 or 110 mm that were 25 mm in diameter. Valve V1 was opened to fluidize the MCC using pure CO_2. The coating was then started by opening valve V2 and closing V1 simultaneously, so as to switch the flow from CO_2 to the solute-laden CO_2 solution. In a similar manner to the RESS-WTS, the solution carried the active through the nozzle, forming a high speed jet into the MCC fluidized bed. The particles of active precipitated from the solution and were collected on the surface of the MCC. After a designated coating time (10 min), the flow of the CO_2 solution reverted to pure CO_2 to purge the pipeline for a further 10 min. The coated MCC particles were stored in the same way as described above in 2.4 for further characterization and analysis.

In both RESS-WTS and RESS-BFB coating procedures the distance between the nozzle and MCC particles in the bed was kept to a minimum, i.e. the fluidized bed was in direct contact with the surface of the gas distributor plate, into which the nozzle was inserted, so that its tip was slightly countersunk (~15 mm) into the plate. The intention here is to capture the active particles close to their point of origin, so restricting subsequent particle growth and aggregation before capture and maintaining them in their nucleated nano-size.

In conventional RESS processes, tuning of the pressure and temperature enables the particle size to be manipulated [7–12], although subsequent growth and aggregation make it difficult to maintain the desired size. In the process described here, the conditions within the fluidized bed can also be used to tune the particle size. In the near/supersonic free jet, the pressure, temperature and supersaturation change very rapidly along the expansion path, so that nucleation can occur within a distance of less than a millimetre from the nozzle tip or even within the nozzle itself [14].

2.6. Material and surface analysis

2.6.1. Quantitative determination of loading

The extent of loading (mg active/g MCC) was measured by quantitatively dissolving the coated sample in an appropriate solvent, measuring the absorbance of the solution at a specific wavelength and comparing the response with a standard curve. The loadings of actives on MCC were then determined by back calculation.

2.6.2. SEM

SEM images were taken using a Philips XL30 ESEM-FEG electron microscope [Philips, Netherlands] fitted with an Oxford Inca 300 EDS system [Oxford Instruments, UK].

2.6.3. EDX

EDX scans were undertaken using a Philips XL30 ESEM-FEG electron microscope fitted with an Oxford Inca 300 EDS system. Ferrocene was the only compound that possesses an element (iron) that was different from the background elements of MCC: hydrogen, oxygen and carbon. EDX was therefore undertaken on ferrocene-coated MCC only.

a) Uncoated MCC (red, left) and benzoic acid coated MCC (lighter red, right)
The coating was processed at CO_2 conditions of 100 bar, 40 °C for 60 minutes

b) Ferrocene coated MCC (yellow, left) and uncoated MCC (white, right)
The coating was processed at CO_2 conditions of 100 bar, 40 °C for 10 minutes

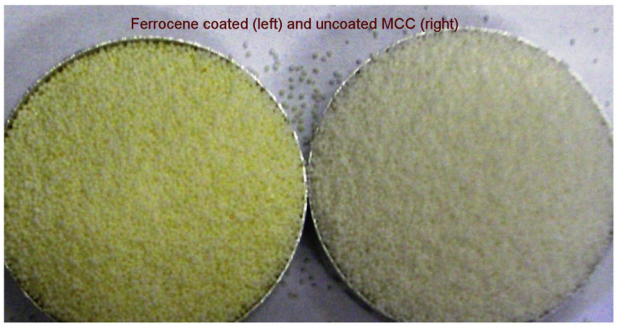

c) Vitamin K_3 coated MCC (yellow, left) and uncoated MCC (white, right)
The coating was processed at CO_2 conditions of 100 bar, 40 °C for 10 minutes

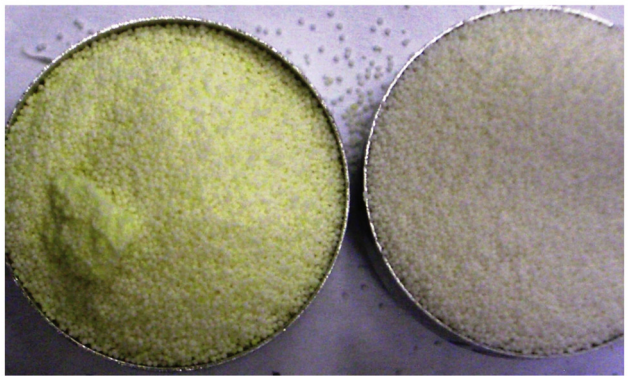

Fig. 2. Gross colour change of MCC samples after RESS-WTS coating.

2.6.4. Confocal Raman spectroscopy

Confocal Raman images were obtained using an Alpha300 Confocal Raman Microscope (WITec, Germany). Firstly, the pure materials were scanned as standards to obtain the standard spectra and characteristic wavenumber peaks. The coated sample was then scanned and the wavenumbers of the standard characteristic peaks were chosen for the instrument to assemble the image. If the active was detected on the MCC, accordingly a region of bright colour would appear on the image. In addition, surface point analysis was also investigated. The point of selection would either be an uncoated region (i.e. MCC) or a coated region (i.e. the active). If the coating was thin then the scan obtained detected characteristic wavenumber peaks of both the active and MCC in the spectra.

3. Results and discussion

3.1. Evaluation of coating achieved using RESS-WTS

3.1.1. Colour-change of coated samples and determination of loading

The colour change of MCC before and after coating in the RESS-Wurster coater was used as a visual indication of the success of the process (Fig. 2). Both the colour change of MCC when coated with coloured actives and the coating of white actives on coloured MCC were evaluated. Fig. 2a–c shows MCC coated with benzoic acid, ferrocene and vitamin K3, respectively. The colour change is obvious and uniform at this scale (colour available only to electronic

Table 1
Quantitative analysis of active loadings on MCC produced by the RESS-WTS process.

Test Active	SuCo-2d Benzoic acid	SuCo-Ad Adamantane	SuCo-Fe Ferrocene	SuCo-Ph Phenanthrene	SuCo-SA Stearic acid	SuCo-VK_3 Vit K3
Loading (mg/g)	3.84	0.12	1.79	3.32	0.60	2.90
Solubility of active in 40 °C CO_2 (g/kg CO_2)	1.898 (100 bar)	0.491 (100 bar)	2.757 (95 bar)	1.310 (107 bar)	0.761 (101 bar)	3.569 (95 bar)

Samples processed at CO_2 conditions of 100 bar, 40 °C using 40 g MCC and 10 min coating time.
Solubility data obtained from Ref. [31].
When there are no data available at 40 °C, an interpolation method was used to estimate the value. When there are a lack of data at 100 bar, the data for the nearest pressure was adopted.

readers of this paper). All samples were processed at the same CO_2 conditions of 100 bar 40 °C except that shown in Fig. 2a where a longer coating time was used (60 min).

Quantitative results are shown in Table 1 as the loading of active (mg) coated onto MCC (g). All tested actives could be coated onto MCC by the RESS-WTS process, clearly showing the potential of the approach. The loading varies from 0.12 to 384 mg/g at the same process conditions and coating time, which indicates that the efficiency of the coating process largely depends on the properties of the active and its solubility in CO_2 because all other parameters remained constant. It was also noted that the loading increased with coating time and also as the overall tendency of solubility increases. For example, when the coating time was increased from 10 to 60 min, the loading increased to 146 mg/g for benzoic acid. Table 1 also shows solute solubility in CO_2 at around 100 bar and 40 °C [31] for comparative purposes.

3.1.2. Surface analysis

The surfaces of the coated samples produced were analyzed using Confocal Raman spectroscopy and all the images show similar results, but to avoid repetition of data, the full results from one active compound (benzoic acid) are shown here to represent the general behaviour. In addition, to assist in comparison a set of SEM images at the same magnification is shown in which all the active coatings are compared.

3.1.2.1. Confocal Raman spectroscopy. Fig. 3 shows the Confocal Raman spectra and images for benzoic acid coated on MCC processed at CO_2 conditions of 100 bar, 40 °C for 10 min. It consists of images of the scan area and spectrum curves. Both images show the same area but track different specific wavenumbers for either MCC or benzoic acid. If the specific wavenumbers are present on the MCC surface their intensity is displayed as an area of increasing brightness. Conversely, if the selected peak is not found this is reflected by an area of darkness in the image. In Fig. 3 the left-hand image tracks signature wavenumbers for benzoic acid, whereas the right-hand image tracks the signature wavenumbers for MCC.

The left-hand image shows the distribution of benzoic acid on the surface of MCC, with benzoic acid-rich areas showing as regions of brightness; as there are only two compounds in the sample being scanned, the dark area would therefore by deduction be the MCC. The image on the right-hand side is the same scan as the left-hand image but shows the regions of signature peak density for MCC. In this image the bright areas show the MCC and the dark areas represent the distribution of benzoic acid on the surface.

The red spectrogram beneath these images show the spectra at the points indicated by the crosses on the images above and the two standard curves of MCC (green) and benzoic acid (blue) for identification and comparison. A comparison of the red sample spectrum with the two standard spectra enables the composition

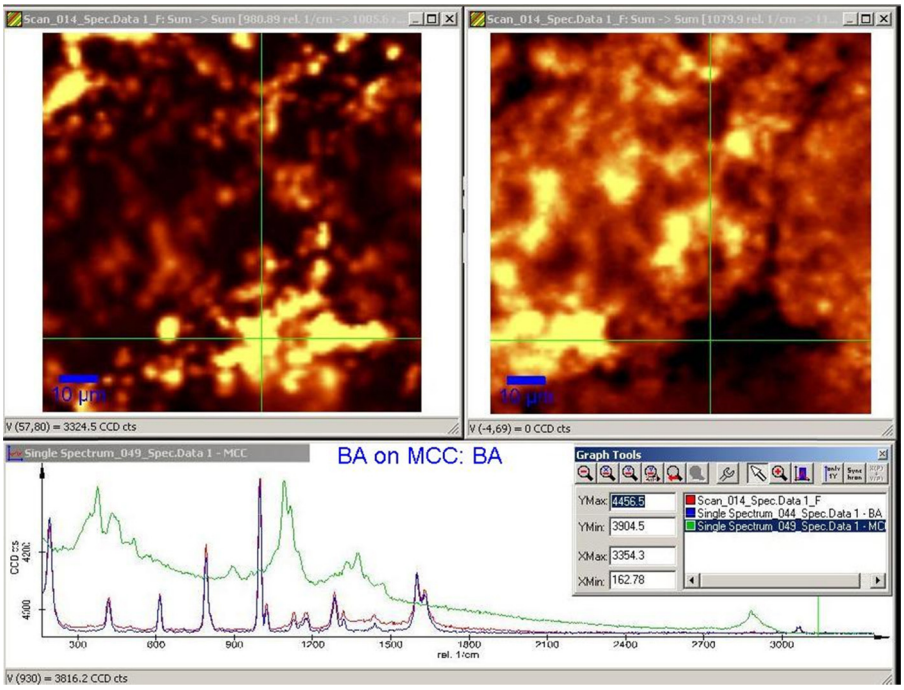

Fig. 3. Confocal Raman analysis of benzoic acid coated on MCC produced by the RESS-WTS.

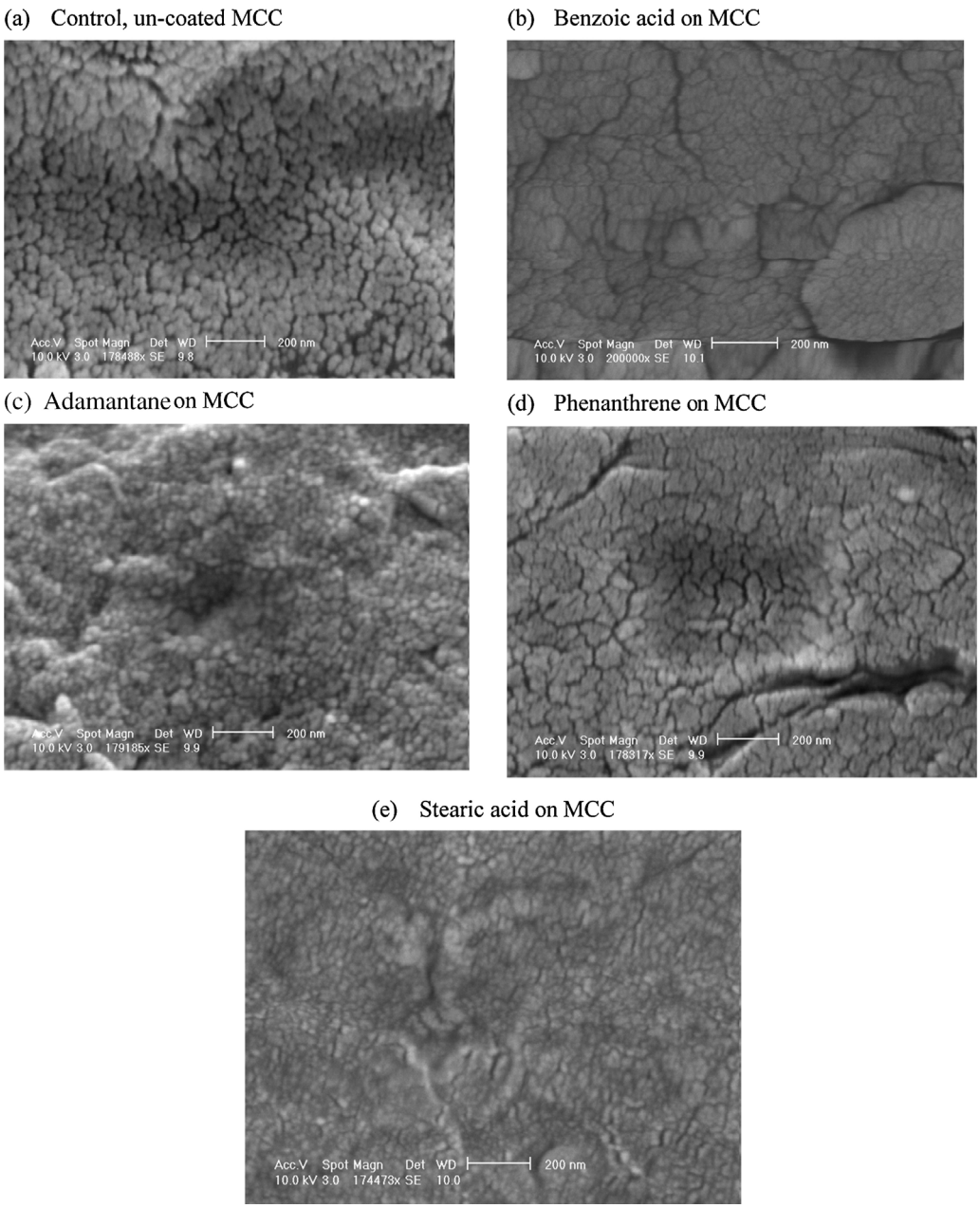

Fig. 4. Scanning electron micrographs of particle surfaces after RESS-WTS coating. The control is MCC alone that has been subjected to the process in the absence of any active (i.e. pure CO_2).

of the surface to be determined. It is clear that the red spectrum almost overlaps the blue benzoic acid standard curve. This provides evidence that benzoic acid was coated on the MCC and was aggregated locally as shown on the confocal image.

It is apparent from the images that the MCC surface is not atomically smooth and this translates to the observed covering of the benzoic acid surface coating, which was preferentially retained in the surface troughs; this is in agreement with the results obtained from SEM analysis. This is also confirmed by scanning a point on the surface where the coating was thinner which gave a spectrum showing evidence of both active and MCC (not shown). Ferrocene, phenanthrene and vitamin K3 on MCC showed similar confocal Raman results, with the distribution of these respective actives on the MCC clearly seen.

In contrast, two actives, adamantane and stearic acid, showed no evidence of coating using confocal Raman analysis. The loading of adamantane on MCC was found to be the lowest in this work at only 0.12 mg/g. The confocal Raman spectroscopy results were therefore inconclusive due to the low loading, though the mass balance and SEM (see below) corroborate that active was present on the MCC surface. Stearic acid has very similar standard feature peaks at wavenumbers very close to those of the MCC standard, and this therefore made it difficult to distinguish stearic acid from the MCC by confocal Raman spectroscopy. Several attempts were made but drew inconclusive results.

3.1.2.2. SEM analysis. The SEM images of coated and control MCC (for comparison) are shown in Fig. 4 In all images the scale bar is 200 nm. The images imply that for all the actives studied the coating on the MCC particles were in the nanosize range. There is evidence on the images that the visible feature size is much below the 200 nm scale bar. In some instances particularly Images 4b and 4d, the coating appeared as a continuous thin layer closely following the undulations of the MCC surface. Although the particle size

Table 2
Quantitative analysis of active loadings on MCC produced by the RESS-BFB process.

Test Active	Tube-BA-40 g Benzoic acid	Tube-BA-60 g Benzoic acid	Tube-Fe-40 g Ferrocene	Tube-Fe-60 g Ferrocene
Loading (mg/g)	5.39	3.78	4.14	3.93

Samples processed at CO_2 conditions of 100 bar, 40 °C and coating for 10 min −40 g and −60 g indicate the respective masses of MCC in the bed, which gave bed depths of 70 and 110 mm.

is below the resolution of the instrument, it is easy to distinguish between the coated and un-coated MCC surfaces. The main observation is that the characteristically rough MCC surface becomes smoother after being coated; imperfections and cracks on the surface are filled. It should be noted that TEM analysis was not possible due to curvature of the surface and desorption of the active from the surface as a result of the increased partial vapour pressure of the active under vacuum of the TEM. Microtomes were also not possible due to the fragile nature of MCC.

3.1.2.3. EDX. As noted earlier, ferrocene was chosen as the active for EDX studies because it contains iron, which is easily distinguishable from the MCC background. An 85 × 425 μm rectangular area was selected and the scan detected there was 0.07 wt% iron on the surface. The loading of ferrocene on MCC was found to be 179 mg/g and the iron content in ferrocene is 30.12 wt%. The calculated iron content (0.054 wt%) therefore agrees reasonably well with the EDX scan result. Furthermore, a point scan on the surface detected a relatively abundant source of ferrocene (0.57 wt%), which was a consequence of the undulated MCC surface preferentially collecting a higher loading of the precipitated ferrocene particles.

3.2. Coating using RESS-BFB

Two actives, benzoic acid and ferrocene were used in these tests. The RESS process conditions were the same as for the RESS-Wurster tests except: the nozzle was heated to around 60 °C, there was no air flow in to the fluidised bed and 40 and 60 g MCC were used. Quantitative analyses of coated MCC are shown in Table 2. The results indicate that the RESS-BFB was able to achieve higher loadings depending on the mass of MCC used and consequently the bed depth. Particles of nano-size will be collected by diffusional mechanisms which are more effective in a deeper bed. Surface analyses of the sample were carried out using the same methods as those used on RESS-WTS samples (SEM, EDX, Confocal Raman) and similar results were obtained. These results indicate the possibility of using the same coating principles but different equipment to achieve similar outcomes, therefore giving more flexibility in the facility design when considering this process.

3.3. Process yield

The intention of this work is to present a coating process that allows the production of nanoparticles and their capture onto larger carriers. At this stage, the results of process yield are not given; however, the process yield depends on the properties of the active and the operation parameters and for the tests presented it ranged from 14% to 74%. It is our intention to report fully the effect of operation parameters on process yield in forthcoming work.

4. Conclusion

The novel RESS-fluidized bed coating process developed in this work combines the principles of supercritical fluid precipitation with those of fluidized bed coating to achieve coatings of nanoparticles onto a micron-sized excipient, for a range of nanoparticle actives. Typically, active loadings in the order of 1–10 mg/g of excipient can be achieved in 10 min. The process avoids the use of liquids and the whole procedure is simpler, faster and easier than conventional coating processes in a Wurster coater. It combines the advantages of both the RESS and fluidized bed processes, by generating nano-particles of organic based compounds by RESS and coating them onto excipient micro-particles. The limitations of this process lie in the solubilities of actives in carbon dioxide.

Acknowledgements

The authors thank the EPSRC (EP/F037228/1) for funding this research and Dr J Bowen for help using the Confocal Raman microscope. The Confocal Raman microscope used in this research was obtained, through Birmingham Science City: Innovative Uses for Advanced Materials in the Modern World (West Midlands Centre for Advanced Materials Project 2), with support from Advantage West Midlands (AWM) and part funded by the European Regional Development Fund (ERDF).

References

[1] G.G. Liversidge, K.C. Cundy, Particle size reduction for improvement of oral bioavailability of hydrophobic drugs: I. Absolute oral bioavailability of nanocrystalline danazol in beagle dogs, International J. Pharmaceutics 125 (1995) 91–97.
[2] X. Zhou, W. Xu, G. Liu, D. Panda, P. Chen, Size-dependent catalytic activity and dynamics of gold nanoparticles at the single-molecule level, J. American Chemical Society 132 (2010) 138–146.
[3] J. Jung, M. Perrut, Particle design using supercritical fluids: literature and patent survey, J. Supercritical Fluids 20 (2001) 179–219.
[4] J.W. Tom, P.G. Debenedetti, Particle formation with super-critical fluids – a review, J. Aerosol Science 22 (1991) 555.
[5] A. Kordikowski, T. Shekunov, P. York, Polymorph control of sulfathiazole in supercritical CO_2, Pharmaceutical Research 18 (2001) 682–688.
[6] A.D. Edwards, B.Y. Shekunov, A. Kordikowski, R.T. Forbes, P. York, Crystallization of pure anhydrous polymorphs of carbamazepine by solution enhanced dispersion with supercritical fluids (SEDS™), J. Pharmaceutical Sciences 90 (2001) 1115–1124.
[7] J. Robertson, D.R. Merrifield, P.C. Buxton, J.P.K. Seville, M.B. King, Generation of powders using supercritical fluids: phase equilibria measurements, the use of the RESS process and its applications to pharmaceuticals, in: Proceedings of the 7th World Congress of Chemical Engineering, Glasgow, 2005.
[8] P.G. Debenedetti, Supercritical Fluids Fundamentals for Application, Kluwer Academic Publishers, Boston, 1994, pp. pp719.
[9] H. Krober, U. Teipel, H. Krause, Manufacture of submicron particles via expansion of supercritical fluids, Chemical Engineering Technology 23 (2000) 763–765.
[10] M. Turk, P. Hils, B. Helfgen, K. Schaber, H.J. Martin, M.A. Wahl, Micronization of pharmaceutical substances by the rapid expansion of supercritical solutions (RESS): a promising method to improve bioavailability of poorly soluble pharmaceutical agents, J. Supercritical Fluids 22 (2002) 75–84.
[11] R.K. Franklin, J.R. Edwards, Y. Chernyak, R.D. Gould, F. Henon, R.G. Carbonell, Formation of perfluoropolyether coatings by the rapid expansion of supercritical solutions (RESS) process. Part 2: Numerical modeling, Industrial & Engineering Chemistry Research 40 (2001) 6127–6139.
[12] P. Pathak, M.J. Meziani, T. Desai, Y.-P. Sun, Nanosizing drug particles in supercritical fluid processing, J. American Chemical Society 126 (2004) 10842–10843.
[13] J.P.K. Seville, U. Tüzün, R. Clift, Processing of Particulate Solids, Chapman & Hall/Kluwer, London, 1997.
[14] P. Hirunsit, Z. Huang, T. Srinophakun, M. Charoenchaitrakool, S. Kawi, Particle formation of ibuprofen – supercritical CO_2 system from rapid expansion of supercritical solutions (RESS): a mathematical model, Powder Technology 154 (2005) 83–94.
[15] A.K. Kulshreshtha, O.N. Singh, G.M. Wall (Eds.), Pharmaceutical Suspensions – From Formulation Development to Manufacturing, Springer-Verlag, New York, 2010, p. 298.
[16] J.P.K. Seville (Ed.), Gas Cleaning in Demanding Applications, Springer, Dordrecht, 1997.
[17] S.C.S. Rocha, O.P. Taranto, in: N. Epstein, Grace J.R. (Eds.), Granulation & particle coating, in Spouted & Spout-Fluid Beds, Cambridge University Press, UK, 2011.
[18] R. Clift, M. Ghadiri, K.V. Thambimuthu, in: R.J. Wakeman (Ed.), Progress in Filtration and Separation, vol. 2, Elsevier, Amsterdam, 1981.
[19] J.H. Kim, T.E. Paxton, D.L. Tomasko, Microencapsulation of naproxen using rapid expansion of supercritical solutions, Biotechnology Progress 12 (1996) 650–661.
[20] K. Mishima, K. Matsuyama, D. Tanabe, S. Yamauchi, T.J. Young, K.P. Johnston, Microencapsulation of proteins by rapid expansion of supercritical solution with a nonsolvent, AIChE 46 (2000) 857–865.

[21] Reverchon, in: A. Bertucco, F. Vaccaro (Eds.), Proceeding of the 4th Italian Conference on Supercritical Fluids and Their Applications, Capri, 1997, pp. 327–334.
[22] R. Falk, T.W. Randolph, J.D. Meyer, R.M. Kelly, M.C. Manning, Controlled release of ionic compounds from poly (L-lactide) microspheres produced by precipitation with a compressed antisolvent, J. Controlled Release 44 (1997) 77–85.
[23] N. Elvassore, A. Bertucco, P. Caliceti, Production of protein-loaded polymeric microcapsules by compressed CO_2 in a mixed solvent, Industrial & Engineering Chemistry Research 40 (2001) 795–800.
[24] Y. Wang, D. Wei, R. Dave, R. Pfeffer, M. Sauceau, J-J. Letourneau, J. Fages, Extraction and precipitation particle coating using supercritical CO_2, Powder Technology 127 (2002) 32–44.
[25] A. Tsutsumi, S. Nakamoto, T. Mineo, K. Yoshida, A novel fluidized-bed coating of fine particles by rapid expansion of supercritical fluid solutions, Powder Technology 85 (1995) 275–278.
[26] T.J. Wang, A. Tsutsumi, H. Hasegawa, T. Mineo, Mechanism of particle coating granulation with RESS process in a fluidized bed, Powder Technology 118 (2001) 229–235.
[27] R. Schreiber, C. Vogt, J. Werther, G. Brunner, Fluidized bed coating at supercritical fluid conditions, J. Supercritical Fluids 24 (2002) 137–151.
[28] R. Schreiber, B. Reinke, C. Vogt, J. Werther, G. Brunner, High-pressure fluidized bed coating utilizing supercritical carbon dioxide, Powder Technology 138 (2003) 31–38.
[29] H. Krober, U. Teipel, Microencapsulation of particles using supercritical carbon dioxide, Chemical Engineering and Processing 44 (2005) 215–219.
[30] S. Palmer, A. Ingram, J.P.K. Seville, The Wurster coater, in: N. Epstein, J.R. Grace (Eds.), Spouted & Spout-Fluid Beds, Cambridge University Press, 2011.
[31] R.B. Gupta, J. Shim, Solubility in Supercritical Carbon Dioxide, CRC Press, London, 2007.